1
2
3
Experimental demonstration of a mode shape-based scour monitoring method for multi-span bridges with shallow foundations

4   Abdollah Malekjafarian, Ph.D. [1], Chul-Woo Kim, Ph.D. [2], Eugene J. OBrien, Ph.D. [3],
5   Luke J. Prendergast, Ph.D. [4], Paul C. Fitzgerald, Ph.D. [5*], Syunsuke Nakajima [6]

6 ## Abstract

7   This paper experimentally investigates a vibration-based scour monitoring approach applicable

8   to bridges with multiple simply supported spans on shallow foundations. A monitoring strategy

9   based on the relative changes in pier mode shape amplitudes due to scour is postulated. The

10   first global mode shape of a bridge structure with multiple spans is extracted from acceleration

11   measurements using an output-only approach, Frequency Domain Decomposition (FDD). The

12   relative changes of the pier mode shape amplitudes under scour are then tracked. Here, each

13   pier mode shape value is compared with the mean values of the remaining piers in a process

14   that creates a Mean-Normalised Mode Shape (MNMS). The approach is demonstrated on a

15   scaled model of a bridge with four spans, supported on sprung foundations, where scour is

16   simulated by the replacement of springs with springs of lower stiffness corresponding to a

17   reduction in foundation stiffness. It is shown that at a given 'scoured' pier, significant increases

18   in the MNMS value occur, suggesting that the location of the scour can be identified. The

19   magnitude of the MNMS at a given pier also increases with an increase in stiffness loss due to

20   scour. In practice, the approach would work best by carrying out a visual inspection of the

[1] School of Civil Engineering, University College Dublin, Dublin, Ireland. Email abdollah.malekjafarian@ucd.ie
[2] Department of Civil and Earth Resources Engineering, Kyoto University, Kyoto 615-8540, Japan. Email kim.chulwoo.5u@kyoto-u.ac.jp
[3] School of Civil Engineering, University College Dublin, Dublin, Ireland. Email eugene.obrien@ucd.ie
[4] Department of Civil Engineering, Faculty of Engineering, University of Nottingham, Nottingham, NG7 2RD, United Kingdom. Email luke.prendergast@nottingham.ac.uk
[5] School of Civil Engineering, University College Dublin, Dublin, Ireland. Email paul.fitzgerald.3@ucdconnect.ie
[6] Department of Civil and Earth Resources Engineering, Kyoto University, Kyoto 615-8540, Japan. Email nakajima.syunsuke.35x@st.kyoto-u.ac.jp

*Corresponding author

21   bridge to establish the initial health condition at the time of sensor installation. After this initial

22   process, the bridge can be monitored remotely for scour on an ongoing basis.

23   **Keywords:** Bridge scour; accelerations; mode shape; damage detection; SHM; vibrations

Introduction

25   Scour erosion, where soil is removed from around bridge foundations by the action of flowing

26   water (Hamill, 1999), remains a significant hazard to bridges worldwide (Wardhana and

27   Hadipriono, 2003, Maddison, 2012, Prendergast et al., 2018). There are three main forms of

28   scour, general, contraction and local. General scour occurs naturally in river channels and

29   includes the aggradation and degradation of the river bed that may occur as a result of changes

30   in the hydraulic parameters governing flow such as changes in the flow rate or changes in the

31   quantity of sediment in the channel (Forde et al., 1999). Contraction scour occurs due to

32   changes in the cross-sectional (flow) area of a river due to the presence of obstructions such as

33   piers or abutments. Local scour occurs in the direct vicinity of a bridge foundation where

34   downward flow is induced at the upstream end of bridge piers, leading to local erosion (Forde

35   et al., 1999).

36   In its simplest form, scour leads to a lowering of the soil elevation relative to foundation

37   elements of a bridge, which can increase the vulnerability to failure. Perhaps a more significant

38   issue occurs for bridges founded on shallow pad foundations, where scour can undermine the

39   pad, decreasing the soil-structure contact area. This leads to increased stress on the remaining

40   soil, increasing soil strains and ultimately reducing the shear stiffness of the soil beneath the

41   foundation system (Oztoprak and Bolton, 2013). This type of scour mechanism is particularly

42   dangerous because many bridges have unknown foundation depths, meaning it is difficult for

43   bridge owners/operators to truly understand scour risk (Briaud et al., 2012).

44   The reduction in foundation stiffness as a result of scour can lead to excessive settlements,

45   which pose issues to bridges and can affect their load-carrying capacity. In terms of load-rating

46   of structures to identify carrying capacity, recent efforts have sought to include foundation

47   settlements into assessment frameworks (Davis et al., 2018).

48   It is widely recognised that scour reduces the stiffness of foundations, which has given rise to

49   the area of vibration-based scour detection (Briaud et al., 2011, Foti and Sabia, 2010,

50   Prendergast et al., 2013, Chen et al., 2014, Klinga and Alipour, 2015, Prendergast et al., 2016a,

51   Xiong et al., 2018b, Kong et al., 2013, Fitzgerald et al., 2019a). The idea that changes in

52   stiffness manifest themselves as changes to modal properties is the original concept behind

53   monitoring dynamic properties for structural damage detection (Sohn et al., 2003). Many

54   researchers have investigated approaches to scour detection based on measuring changes in

55   various dynamic properties using sensors installed on the superstructure, or on passing vehicles

56   (Fitzgerald et al., 2019b). These studies include both numerical and experimental

57   investigations, and the majority of studies to date have focussed on bridges with deep

58   foundations (piles). For a comprehensive overview of approaches based on changes in natural

59   frequencies, interested readers are referred to Bao and Liu (2017).

60   Using numerical modelling, Prendergast et al. (2016a, 2016b) investigate how scour around

61   the central pier of a two-span integral bridge influences the first natural frequency of the

62   structure and study the ability to use changes in this frequency to detect scour. The influence

63   of parameters such as vehicle speed and mass, road surface roughness and sensor 'noise', on

64   the resulting lateral pier vibrations are studied to ascertain how robust the approach is for scour

65   detection. They conclude that monitoring frequency changes shows potential to detect scour

66   erosion. The approach is extended in Prendergast et al. (2017) to detecting the location of scour

67   on a two-span integral bridge, i.e. which pier or abutment is scoured, by analysing multiple

68   frequencies from the bridge with a focus on local element frequencies. Kong and Cai (2016)

69 numerically investigate the dynamic response of a continuous four-span bridge under wave

70 loads and demonstrate that scour has a significant effect on the lower frequencies of a bridge

71 pile. Furthermore, it is shown how scour affects the complete bridge-vehicle-wave system,

72 meaning that the response of the bridge deck or even a passing vehicle can also be used to

73 monitor scour. Ju (2013) studies how the natural frequency of a bridge varied due to scour

74 using numerical modelling. It is shown how water-added mass surrounding the foundations

75 influences the frequency values and it is concluded that its presence lowers the frequency.

76 However, accounting for water-added mass is difficult and it is recommended that it can be

77 ignored in bridge frequency analyses. Chen et al. (2014) present a scour monitoring approach

78 using velocity sensors and a finite-element model of a cable-stayed bridge. Combining sensor

79 measurements with FE updating enables scour of the pier to be quantified. Klinga and Alipour

80 (2015) perform numerical analyses on the performance of various bridge elements under

81 extreme scour and conclude that scour reduces lateral stiffness and lowers the natural

82 frequency. Xiong et al. (2018a) propose a scour indicator based on the bridge flexibility matrix,

83 which is sensitive to scour-induced changes on the frequencies and mode shapes of the

84 structure. Bao et al. (2017) perform numerical and experimental studies to investigate three

85 particular issues with frequency-based scour detection, namely (i) the physical meaning of the

86 predominant natural frequency (PNF), (ii) the optimal location for installed sensors, and (iii)

87 the influence of scour hole shape. By comparing a modal PNF to one obtained from dynamic

88 testing, separation of bridge (structural) frequencies and soil (or computational domain)

89 frequencies is possible. In terms of optimal sensor location, they suggest locating sensors at a

90 point near maximum modal amplitude. For the structure considered in their paper, this is the

91 top of the pier (free end). Furthermore, they propose a new criterion to define scour depths in

92 asymmetrical scour situations to ensure a smooth variation of PNF with scour.

93   Several authors have trialled other types of (non-frequency) vibration-based scour detection

94   methods on both laboratory-scale and full-scale bridges. Foti and Sabia (2010) present a study

95   on a full-scale five span bridge where one of the piers experienced historical scour issues. By

96   monitoring the asymmetric dynamic behaviour of the pier (due to variations in upstream and

97   downstream scour) using the covariance of accelerations measured by an array of sensors along

98   the foundation, they conclude that scour presence is detectable (but the extent is not

99   quantifiable). Briaud et al. (2011) undertook experimental testing on a scaled-model bridge and

100   investigated the performance of a range of approaches at detecting scour. One particular

101   approach was to analyse the root-mean-square of acceleration signals measured in various

102   directions and to use this as an indicator of scour occurrence. The ratio of RMS values showed

103   sensitivity to scour development (Prendergast and Gavin, 2014).

104   The use of mode shapes to detect scour is a relatively recent development. However, mode

105   shapes have been used in other damage detection fields to detect general forms of structural

106   damage (cracks etc.). Damage detection methods based on changes in mode shapes are an

107   alternative to natural frequency-based approaches, and can be advantageous in detecting local

108   damage, and are not as prone to issues such as changes in temperature (Sohn, 2006). Structural

109   damage detection using mode shapes generally consists of either comparing two modes from

110   different health states of the structure, extracting features of the mode shape (e.g. curvature)

111   that are sensitive to damage, or applying signal processing techniques to mode shape data (Fan

112   and Qiao, 2011). Two common methods to compare shapes are Modal Assurance Criterion

113   (MAC) and Coordinate Modal Assurance Criterion (COMAC) (Allemang and Brown, 1982,

114   Dos Santos et al., 2000). MAC is a measure of the correlation between two modes with a value

115   of unity representing a perfect match and a value of zero representing no match between the

116   two modes. Hence, a reduction in MAC value may indicate the presence of damage. Salawu

117   and Williams (1995) test MAC on mode shapes obtained from a concrete bridge before and

118   after repair and find that the MAC values change significantly in comparison to the measured

119   frequency changes. COMAC is a pointwise comparison of two mode shapes, with a low

120   COMAC value indicating possible damage at that point. Frýba and Pirner (2001) use COMAC

121   in the repair of a segmentally constructed pre-stressed concrete bridge and show that the

122   COMAC analysis of a repaired segment was similar to that of an undamaged segment.

123   Pandey et al. (1991) show, using an analytical model, that the mode shape curvature (i.e. the

124   second derivative of the mode shape) can detect damage in both a simply supported beam and

125   a cantilever beam. Wahab and De Roeck (1999) use a mode shape curvature-based method on

126   the Z24 bridge in Switzerland and develop an indicator based on the difference in curvatures

127   before and after damage. Other authors have shown, however, that mode shape curvatures are

128   poor for detecting smaller amounts of damage (Ratcliffe, 2000). More detailed reviews of other

129   approaches using mode shapes are depicted in (Carden and Fanning, 2004, Fan and Qiao, 2011,

130   Moughty and Casas, 2017, OBrien and Malekjafarian, 2016, Malekjafarian and OBrien, 2017,

131   Kong et al., 2017).

132   Some previous studies have used mode-shape based approaches to detect and monitor scour

133   erosion. Elsaid and Seracino (2014) investigate the influence of scour on a scaled model of a

134   coastal bridge. Scour is modelled as an increase in the effective length of bridge piles extending

135   from the deck. Mode shape curvature, flexibility-based deflection and flexibility-based

136   curvature are assessed to ascertain their performance at scour monitoring. The study concludes

137   that horizontally-displaced mode shapes show sensitivity to the modelled scour. Moreover, the

138   change in the mode shape curvature, flexibility-based deflections and curvatures showed

139   promise in identifying the existence, location and possibly the extent of scour. Xiong et al.

140   (2018b) investigate four scour indicators for a scoured cable-stayed bridge, namely frequency

141   change ratio, MAC, modal curvature and flexibility-based deflection. Flexibility-based

142   deflection is recommended as the most practical way to detect scour. In a separate study, Xiong

143   et al. (2019) present a scour identification approach based on measuring the ambient vibration

144   of the superstructure of a cable-stayed bridge. By analysing the change in the mode shapes at

145   two different times, qualitative scour identification is possible. The authors furthered the

146   procedure to enable quantitative scour identification using a companion FE model of the

147   system, whose soil stiffness is updated to match the real system.

148   The majority of previous works on vibration-based scour monitoring have focussed on changes

149   in natural frequencies to detect scour presence. Approaches using mode shapes have generally

150   focussed on direct comparison of pre- and post-scour modes using MAC-type analyses or have

151   used modal curvature and flexibility-based deflection. The majority of these studies have been

152   applied to cable-stay bridges or bridges with piled foundations. The contribution of the present

153   work relates to the use of information from the mode shape as identified from output-only

154   modal identification to detect local reductions in stiffness resulting from scour-related stiffness

155   losses. The approach developed is applicable to vertical stiffness loss experienced at shallow

156   foundations, since a majority of previous works have focussed on identifying changes in lateral

157   stiffness as would be expected at deeper foundations. Furthermore, the approach is

158   demonstrated in this paper using scaled experimental testing. The first global mode shape of

159   an experimentally scaled bridge with multiple spans is extracted using Frequency Domain

160   Decomposition (FDD) (Brincker et al., 2001). Accelerations from the bridge midspans and

161   piers are used as the input to the FDD algorithm, arising due to a model vehicle traversing the

162   structure.

163   A novel scour indicator is proposed whereby the mode shape amplitude at one pier is compared

164   to the mean of the mode shape amplitudes at the remaining piers in a process that creates a

165   Mean-Normalised Mode Shape (MNMS). It is shown that at the scoured pier, the MNMS value

166   increases due to a loss of stiffness as a result of scour. Moreover, the magnitude of the MNMS

167   at a scoured pier increases with further decreases in stiffness. The approach is also capable of

168   detecting which pier is scoured by considering the nature of the changes in the MNMS. The

169   MNMS approach is an improvement on using the mode shape of the system alone, as it is more

170   sensitive to scour than changes in mode shape obtained from MAC analysis. Moreover, only

171   one mode shape is required, namely the damaged mode shape, to derive the required

172   information. This means that a reference (undamaged) mode shape is not required, as would

173   be the case when comparing modes using MAC. The method only requires sensors located at

174   piers so does not suffer from the requirement of many sensors, as would be needed for accurate

175   estimates of modal curvature, for example. The method may be suited to output-only scour

176   identification for multi-span bridges founded on shallow pad foundations, which typically have

177   not received much attention in the literature.

178 # Scour monitoring approach based on pier mode shape values

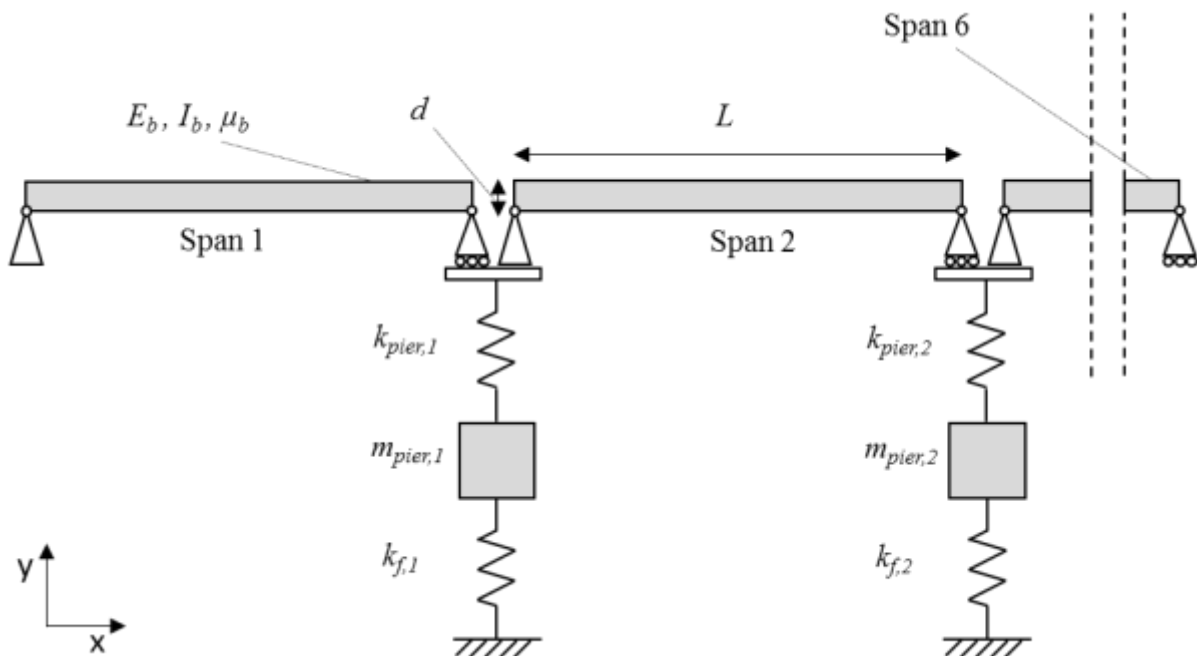179 ## Numerical Model

180

181 Fig. 1: Numerical model schematic

182   A numerical model is used to introduce the scour detection procedure and a schematic of this

183   is shown in Fig. 1. It represents a bridge with pinned connections (internal hinges) between

184   each of six spans. Each pier is assumed to rest on a shallow pad foundation with underlying

185   soil stiffness. Each span is modelled as a simply supported Euler-Bernoulli beam, the mass and

186   stiffness matrices for which are available in (Kwon and Bang, 2000). The beginning and end

187   of the bridge are assumed to rest on undeformable abutments, which are modelled as pinned,

188   and roller supports, respectively. Hence, there are five internal piers. Twenty 1 m long beam

189   elements are used for each span in the finite-element model. The beams are connected using

190   nodal hinges with a supporting pier at each connection, modelled as a single degree of freedom

191   (DOF) sprung-mass in the vertical direction.

192   Each pier is supported by a spring, k_f, which represents the vertical stiffness provided by a

193   shallow pad foundation with notional length, L and width, B dimensions of 4 m and 2 m

194   respectively. Using these pad dimensions, the stiffness of the spring is calculated using the

195   approach in FEMA (2000), see Eq. (1),

$$k_f = \frac{GB}{1-v}\left[1.55\left(\frac{L}{B}\right)^{0.75} + 0.8\right]$$

196   (1)

197   where G is the operational shear modulus of the soil (kN m^{-2}) and v is the small-strain Poisson

198   ratio. An elastic modulus, $E = (2G(1+v))$, corresponding to a medium dense sand (Prendergast

199   and Gavin, 2016) is assumed for the unscoured stiffness. Note, the expression in Eq.(1) is semi-

200   empirical and there exists several formulations that take this approximate form (Pais and

201   Kausel, 1988, Mylonakis et al., 2006). Table 1 lists the main geometrical and material

202   properties of the bridge. The second moment of area is calculated by assuming a 4 m wide

203   single-track railway bridge with a rectangular cross-section and the mass and stiffness of the

204   pier is calculated by assuming pier dimensions of 7 m (in y-direction), 1 m (in x-direction) and

205 2.5 m (into page) with a modulus of elasticity and density of 35×10^6 kN m^{-2} and 2400 kg m^{-3}

206 respectively.

207 Table 1: Properties of bridge used to introduce the scour identification approach

Property	Symbol	Unit	Value
Span length	L	m	20
Beam depth	d	m	1
Beam second moment of area	I_b	m^4	0.33
Beam modulus of elasticity	E_b	kN m^{-2}	35×10^6
Beam mass per unit length	μ_b	kg m^{-1}	9.60×10^3
Pier mass	m_{pier}	kg	42×10^3
Pier stiffness	k_{pier}	kN m^{-1}	12.50×10^6
Vertical stiffness provided by shallow pad foundation	k_f	kN m^{-1}	344.12×10^3

208

209 In this work, scour is modelled as a reduction in stiffness of a given vertical foundation spring.

210 It is worth noting that in the real case a loss of rotational stiffness could occur as a result of

211 scour which would result in rocking effects on the pad. This type of situation could arise in the

212 case of asymmetric scour affecting the foundation (Foti and Sabia, 2010). However, the present

213 study specifically focuses on vertical stiffness loss only (Eq. 1). The basis for scour-related

214 stiffness loss lies in the stress and strain dependency of soil stiffness, as discussed herein. The

215 shear modulus of soil (*G*) typically increases nonlinearly with mean effective stress. The

216 magnitude of this shear modulus at a given depth is a function of the amount of overburden

217 pressure at that location. Scour leads to a local reduction in soil elevation relative to a

218 foundation, which implies the overburden pressure reduces in the vicinity of scoured

219 foundations (Zhang et al., 2017). It can therefore be assumed that scour occurrence would

220 change the operational shear modulus at formation level, although by a small amount. In

221 extreme cases, however, scour can undermine a shallow pad (Scozzese et al., 2019). When this

222 occurs, the contact area between the remaining soil beneath the shallow foundation and the pad

223 is reduced, leading to increased stress on the remaining soil from the applied loads. This

224   increased stress subsequently increases the strain in the soil, due to the typically nonlinear

225   stress-strain relationship of soil. Additionally, the shear modulus of soil is strain-dependant,

226   and typically reduces with strain (Oztoprak and Bolton, 2013, Hardin and Drnevich, 1972). In

227   this paper, both the aforementioned mechanisms are assumed to occur leading to a reduction

228   in the vertical stiffness of a foundation under scour. For the geometries considered in the

229   present study, a 30% example loss in stiffness would be expected if the foundation was

230   undermined by scour reducing the soil-foundation contact area from 8m^2 (4m x 2m) to 5.1m^2

231   (3m x 1.7m), with a corresponding reduction in soil shear modulus, G equating to 10%

232   reduction from the small-strain value G_0 (Oztoprak and Bolton, 2013).

233
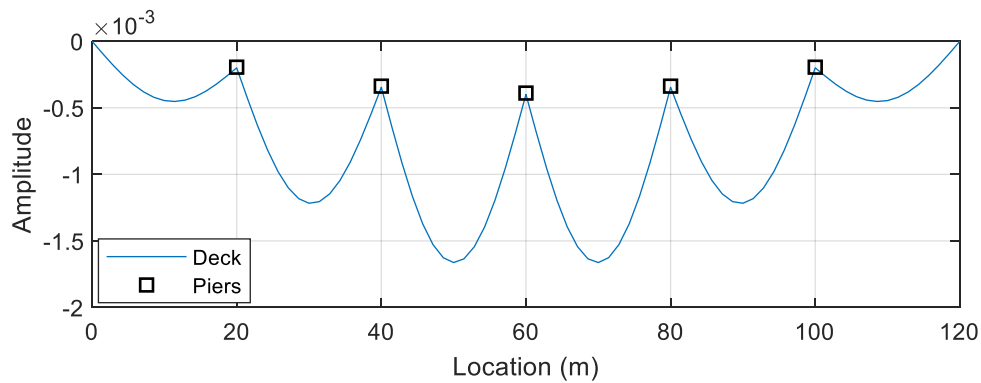
Fig. 2: First mode shape of system for healthy case - 3.70 Hz frequency

235   Fig. 2 shows the first global mode shape of the bridge corresponding to the first natural

236   frequency of the system when there is no scour. The mode shape is derived from the system

237   mass and stiffness matrices by solving the Eigenproblem (Clough and Penzien, 1993). As is

238   evident, each of the bridge spans exhibit a bending shape with each of the piers exhibiting

239   motion in the same direction for this mode. The central pier has the highest maximum mode

240   shape amplitude relative to the remaining piers. The first mode shape of the bridge will be used

241   to develop a scour monitoring approach by investigating the sensitivity of this mode to scour

242   at various locations.

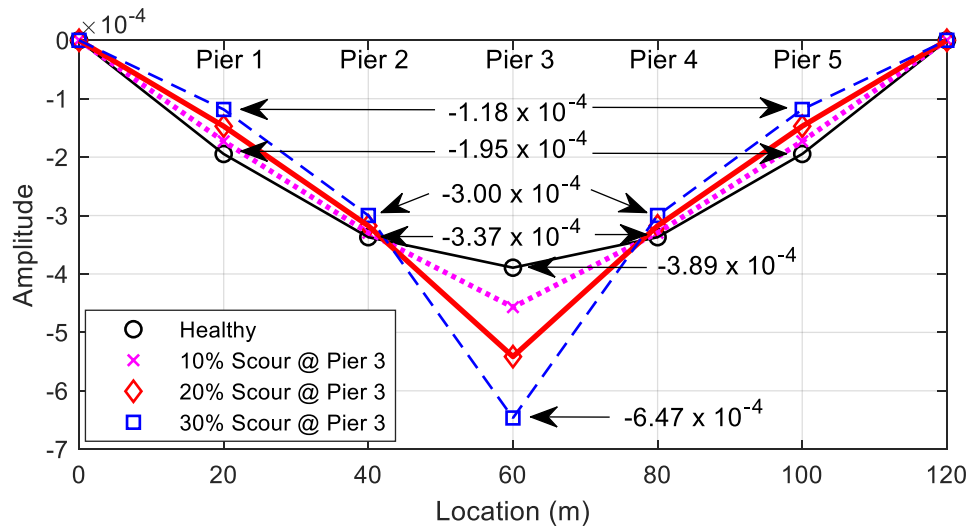## Mean-Normalised Mode Shape (MNMS) to detect Scour

Fig. 3: First mode shape amplitude at pier locations of bridge system due to varying levels of stiffness loss as a result of scour at Pier 3 (60 m point).

Fig. 3 shows how the stiffness loss due to scour affects the first mode shape of the system for

scour at the central pier of the bridge. In this plot, the percentage scour refers to percentage

stiffness loss as a result of scour, and is defined as the reduction in vertical foundation stiffness

with respect to the stiffness of a foundation with zero scour. Only the mode shape values at the

pier locations are shown here and the spans are simplified as straight lines. For each scenario,

the modes are normalised with respect to the system mass matrix so that they can be

quantitatively compared. In this work, a scour indicator based on the first mode shape

amplitudes at the locations of the piers is proposed. The first mode shape is used to develop the

scour indicator because for this mode, all of the piers exhibit movement in the same direction

enabling a ratio-type indicator to be created. Fig. 3 shows that the largest change in the mode

shape amplitude occurs at the scoured pier. It is of note that the mode shape amplitude is

affected at unscoured piers also. At the scoured pier the absolute value of the modal amplitude

increases with an increase in scour (reduced stiffness). At unscoured piers, the opposite effect

is observed whereby the absolute value of the amplitude decreases with an increase in scour. It

should be noted that the changes at the scoured pier are much greater than those at the

12

262   unscoured piers. Based on this premise, a scour indicator referred to as the Mean Normalised

263   Mode Shape (MNMS) is proposed to compare the mode shape value of a given pier with those

264   at the other piers. The mean value of the modal amplitudes of the remaining piers is used as

265   the metric to compare each pier mode shape value. In mathematical form, the MNMS at any

266   pier is represented as Eq. (2).

267
$$\{MNMS\}_x = \frac{\{MS\}_x}{\dfrac{1}{n-1}\displaystyle\sum_{\substack{k=1 \\ k \neq x}}^{n}\{MS\}_k} \tag{2}$$

268   where n is the total number of piers, which in this case is equal to five, x is the pier number

269   such that x $\in$ {1:n}, *MS* is a vector of pier mode shape amplitudes and the summation term

270   represents the sum of the pier mode shape amplitudes excluding Pier x.
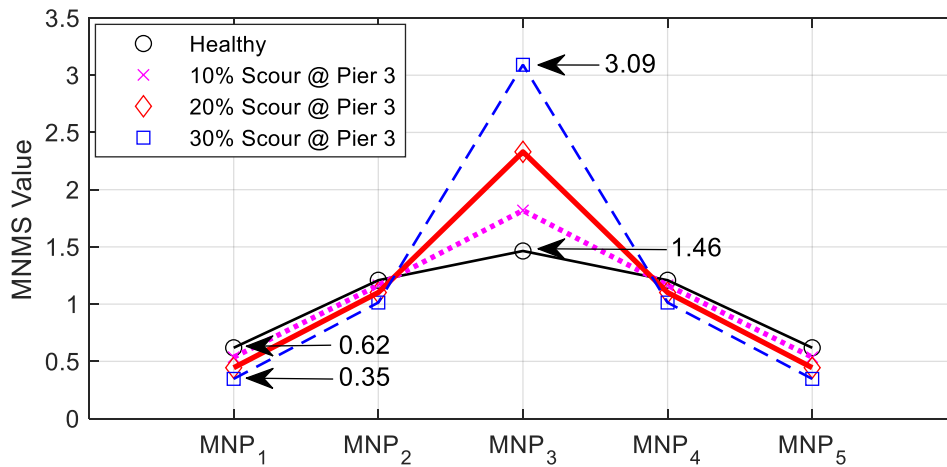
271

272   Fig. 4: MNMS values for each pier for varying levels of scour at Pier 3

273   Fig. 4 shows how the MNMS at each pier is affected by the stiffness loss due to scour at Pier

274   3. At the scoured pier (Pier 3), the MNMS increases with an increase in scour severity from

275   1.46 when there is no scour affecting the bridge to 3.09 when scour corresponding to a 30%

276   decrease in Pier 3 foundation stiffness affects the structure. At other (unscoured) piers, the

277   MNMS values decrease with an increase in scour severity at Pier 3. For example, the MNMS

278   value at Pier 1 decreases from 0.62 to 0.35 where there is 30% scour at Pier 3.

279   It is clear that the MNMS pattern (Fig. 4) has a strong resemblance to the mode shape values

280   themselves (Fig. 3). The main advantage of using the MNMS over direct mode shape

281   comparison lies with the fact that for mode shapes, normalisation is required to facilitate

282   comparison. The mode shapes derived from an output-only modal method like FDD are not

283   mass-normalised as the input forces are unknown (Khatibi et al., 2012). This means that the

284   magnitude of the mode shape values depends on the amplitude of the input forces. For example,

285   a passage of a heavy vehicle may generate signals with higher modal amplitudes than a lighter

286   vehicle. The normalisation process could affect the observed changes due to scour. A common

287   practice for depicting operational mode shapes is to normalise them with respect to their

288   maximum value (Khatibi et al., 2012). However, normalising the mode shapes in this way

289   could lead to a situation where the modes exhibit no change at the location of the scoured pier

290   – which would be the case in Fig. 3. The metric defined in Eq. (2) avails of the relative changes

291   in the mode at various points, therefore it is insensitive to changes in modal magnitude resulting

292   from the passage of different vehicles.
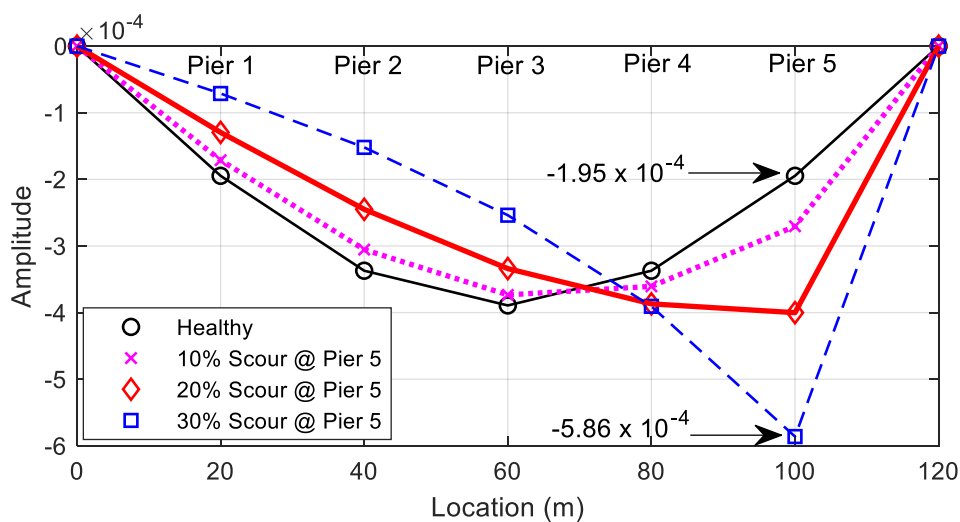

293

294   Fig. 5: First mode shape amplitude at pier locations of bridge system due to varying levels of stiffness loss as a
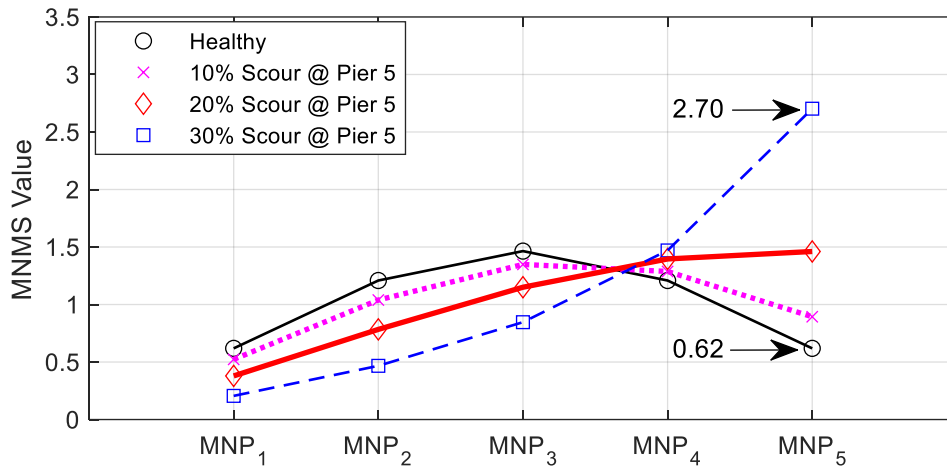295   result of scour at Pier 5 (100 m point).

Fig. 6: MNMS values for each pier for varying levels of scour at Pier 5

Fig. 5 shows how increasing stiffness loss at Pier 5 influences the mode shape amplitudes at each pier. Fig. 6 shows the corresponding MNMS values at each pier. The MNMS values defined in Eq. (2) experience a greater percentage change at the scoured pier than the raw mode shape values at this location (335% as opposed to 200% for the 30% scour case). Note also that the mode shapes in this case are mass-normalised mode shapes directly from Eigen-analyses. In the real case, they would have to be computed from time domain data, making them less reliable. Fig. 6 exhibits a broadly similar trend to that of Fig. 4 in that at the scoured pier, the MNMS value increases while at the unscoured piers it decreases. However, in this case, Pier 4 which is closest to the scoured pier also exhibits an increase in MNMS value. The mode shape itself also reflects this (see Fig. 5) as both Piers 4 and 5 show an increase in absolute mode shape value due to scour at Pier 5.

Frequency Domain Decomposition (FDD)

It is not possible to extract the mode shapes using an eigenvalue analysis on a real structure. Instead, it is necessary to derive modal information by analysing time-domain signals measured from a target structure. In this work, Frequency Domain Decomposition (FDD) (Brincker et al., 2001) is used as a means to extract mode shapes from acceleration measurements. FDD is an output-only modal identification method, i.e. it enables estimation of the system dynamic

15

315   parameters without prior knowledge of the input excitation. The approach is suitable for a

316   scenario where a bridge is excited by unknown vehicle properties.

317   FDD begins with the estimation of the power spectral density (PSD) matrix, $\hat{G}(j\omega)$, from the

318   various responses at discrete frequencies for $\omega=\omega_i$. Next, $\hat{G}(j\omega)$ is decomposed at each

319   frequency by applying Singular Value Decomposition (SVD) (Brincker et al., 2001) to obtain

320   Eq. (3).

$$\hat{G}(j\omega_i) = U_i S_i U_i^H$$ (3)

321

322   where U_i is a unitary matrix of singular vectors, S_i is a diagonal matrix holding the singular

323   values and H denotes the complex conjugate of the matrix. Using the singular values obtained

324   at each frequency, an SVD diagram can then be plotted. From this plot, the natural frequencies

325   of the structure can be obtained from the dominant peaks and the corresponding singular

326   vectors are the mode shapes.

Minimum stiffness loss that can be detected by the MNMS approach under noisy conditions

329   It is of interest to assess the minimum stiffness loss that can be detected by the approach

330   postulated in this paper. To investigate this, a time-domain analysis is conducted whereby the

331   external excitation is by means of a simulated quarter car crossing the bridge model described

332   previously. A quarter car (with two degrees of freedom and crossing speed of 80 km/h) is

333   coupled with the bridge model to form a vehicle-bridge interaction (VBI) model (Keenahan et

334   al., 2013, OBrien et al., 2017) and properties of the quarter car are taken from the literature

335   (Fitzgerald et al., 2019b). Forced vibration data and 5s of free vibration pier acceleration data

336   extracted from the VBI model is inputted to the FDD algorithm from which the mode shapes

337   are extracted. Before they are inputted into the FDD algorithm, noise is added to the clean

338   acceleration signals from the model to generate more realistic accelerations. Random noise is

339   added to the acceleration signals using Eq. (4):

340
$$\{a\} = \{a_{calc}\} + E_p \{N_{noise}\}\{a_{max}\}$$
(4)

341   where a is the noisy acceleration signal, E_p is the level of noise, N_{noise} is a normally distributed

342   vector with a standard deviation equal to one, a_{calc} is the clean acceleration signal outputted

343   from the VBI model and a_{max} is the maximum value of the signal. The level of noise is chosen

344   to be 5%, which is consistent with values used in the literature (Zhu and Law, 2002,

345   Malekjafarian and OBrien, 2014). Keeping the same excitation source, the mode shape

346   extraction process is repeated 10 times, each for a healthy bridge case, and seven scour

347   scenarios ranging from a 2.5% to 17.5% stiffness loss at the central bridge pier. The MNMS is

348   calculated for each run in every scenario, enabling mean and standard deviations of MNMS

349   values to be obtained for each case. Fig. 7 shows an error bar plot (mean +/- one standard

350   deviation) for the MNMS value of the central pier. It can be seen that there are overlaps in the

351   error bars for the lower stiffness loss cases and the healthy case (0% stiffness loss). At around

352   7.5% stiffness loss, there is a clear distinction relative to the error bars of the healthy case.

353   However, the error bars for stiffness losses between 2.5% and 12.5% show an overlap with one

354   another. This suggests that a more realistic estimation for the minimum stiffness loss that can

355   be detected would be greater than 10%. Here, for differences of 12.5%, there are no overlaps
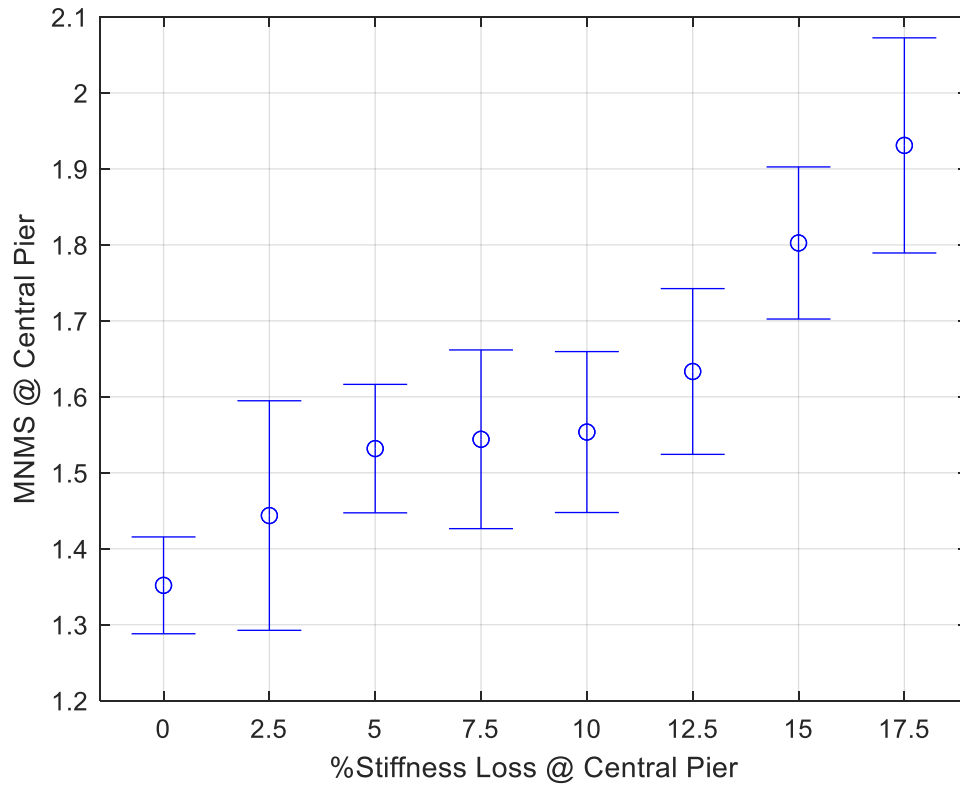
356   between the error bars.

Fig. 7: Minimum scour detectable considering natural variation due to noise of MNMS

Experimental Model

The previous sections introduced the concept of MNMS and demonstrated it via numerical

modelling. In this section, a scaled model of a bridge with multiple simply supported spans has

been developed to experimentally validate the MNMS concept. The tests were conducted in a
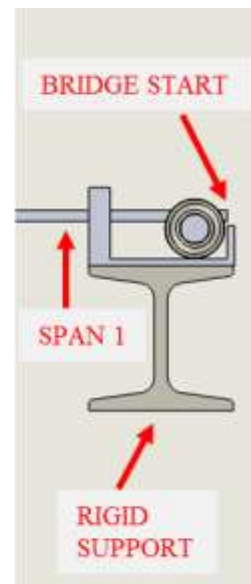
laboratory at Kyoto University in Japan.

364 **Bridge**

(a)

365

(b)   (c)

366
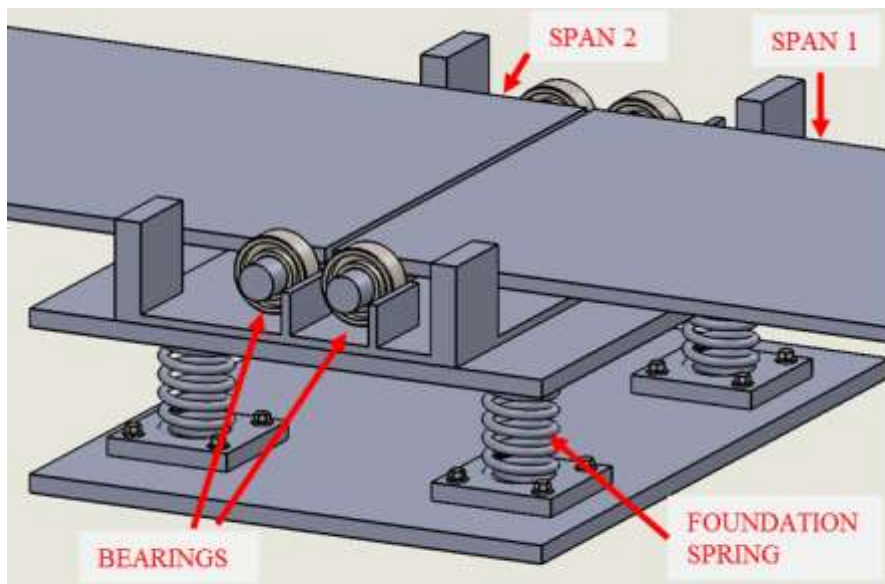
367   Fig. 8: Experimentally scaled multi-span bridge (a) full bridge (b) pier supported on four springs (in this case
368   Pier 1) (c) rigid support at bridge extremes

369   The model bridge consists of four spans supported on three piers - see Fig. 8(a). The bridge

370   was traversed by a scaled model vehicle to generate the external excitation. Each pier was

371   founded on four springs of equal stiffness, to provide vertical stability, and bearings were used

372   to create pin and roller supports (Fig. 8(b)). The start and end of the bridge rest on rigid supports

373   and do not deflect (Fig. 8(c)). Table 2 provides the properties of the beam used for each bridge

374   span.

375   Table 2: Span details

Property	Unit	Value
Span length	mm	1300
Width	mm	300
Beam depth	mm	8.07
Second moment of area (rectangular cross section)	m^4	1.31×10^{-8}
Modulus of elasticity	N m^{-2}	2.05×10^{11}
Density	kg m^{-3}	7850

376

377   The stiffness of the foundation springs was determined from load-displacement testing and

378   benchmarked against geotechnical analyses assuming small-strain linear behaviour, which is

379   appropriate for bridges traversed by moving vehicles. Spring values were defined for the scaled

380   model and a scaling criterion was applied to check compliance at full-scale dimensions, as

381   described herein. The stiffness of each spring used in the experiment (for the healthy bridge

382   scenario) is 49 N mm^{-1}. As four springs were used in parallel beneath each pier, the

383   experimental equivalent stiffness under each support, $k_{f,EXP}$, was 196 N mm^{-1}. In order to

384   achieve compliance with an equivalent full-scale model, a scaling criterion is defined as the

385   ratio of (i) the midspan deflection of a simply supported beam with a unit static load applied

386   directly at midspan, and (ii) the deflection of the support spring when a unit static load is

387   applied directly over a pier. In the numerical model employed to introduce the procedure in the

388   previous section, the stiffness of the pier (k_{pier}) is greater than the foundation stiffness (k_f) by a

389   factor of 36. Therefore, in this criterion the equivalent stiffness of the two in series is governed

390   by the stiffness provided by the shallow pad foundation.

391   In mathematical form, the midspan deflection of a simply supported beam due to a static unit

392   load at the centre is shown in Eq. (5)

393
$$d_{mid} = \frac{L^3}{48EI}$$
(5)

394   where L is the beam span length, E is the Young's Modulus and I is the beam second moment

395   of area. The deflection at a pier, d_{pier}, due to a unit static load immediately overhead, is simply

396   the reciprocal of the stiffness provided by the shallow pad foundation (i.e. $1/k_f$). By maintaining

397   the ratio of d_{mid} to d_{pier} between a full-scale numerical model and the scaled experiment, the

398   experimental foundation stiffness can be represented as Eq. (6)

399

$$k_{f,EXP} = k_{f,NUM} \left(\frac{L_{NUM}^3 E_{EXP} I_{EXP}}{L_{EXP}^3 E_{NUM} I_{NUM}} \right) \qquad (6)$$

400   where subscripts *EXP* and *NUM* denote the experimental and numerical full scaled model

401   respectively.

402   Using the scaling criterion defined in Eq. (6) and taking values of L, E and I from Tables 1 and

403   2, the stiffness provided by an equivalent shallow pad foundation in a full-scale case, $k_{f,NUM}$, is

404   calculated to be 234×10^3 kN m^{-1}. In order to check the validity of this assumption, a

405   benchmark geotechnical case is considered. Using the approach in Fitzgerald et al. (2019b) and

406   FEMA (2000), and taking appropriate values for sand shear modulus from Prendergast and

407   Gavin (2016), the stiffness provided by a shallow pad foundation of length, 4 m and width, 2

408   m is 172×10^3 kN m^{-1} for a loose sand and 344×10^3 kN m^{-1} for a medium dense sand. The

409   scaled experimental spring stiffness used in the present study lies within this range and can

410   therefore be understood to represent a loose to medium dense uniform sand deposit. The mass

411   of each pier, m_{pier}, was 12.56 kg, obtained from measuring the approximate volume of steel

412   directly above the four springs.

413

(a)

(b)

414
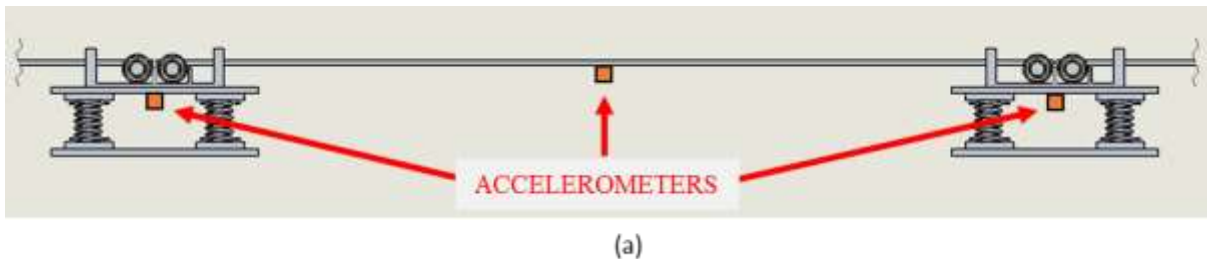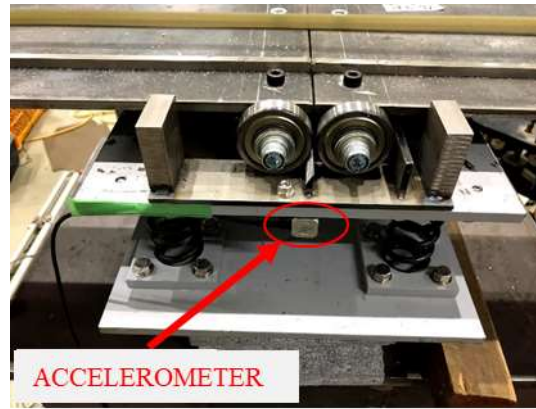
Fig. 9: Accelerometer locations (a) schematic of positions on midspan and pier (b) picture of one pier

416 Accelerometers were installed on each of the piers and at the midspans (Fig. 9). Seven bridge

417 acceleration measurements were recorded ($3 \times$ Piers and $4 \times$ Midspans). Optical sensors were

418 also installed at the beginning and end of the bridge, enabling the timing of when each vehicle

419 axle arrived and departed the bridge be obtained. To model the reduction in stiffness due to

420 scour at a pier, the springs under the pier (Figs. 8(b), 9(b)) were replaced with four springs of

421 a lower stiffness value for a given scour case. Two scour cases were considered, Case I where

422 parallel springs, each of stiffness 37 N mm^{-1}, were used and Case II where parallel springs with

423 stiffness of 27 N mm^{-1} were used. These cases equated to 24.5% and 44.9% stiffness reductions

424 from the healthy case where each parallel spring had a stiffness of 49 N mm^{-1}.
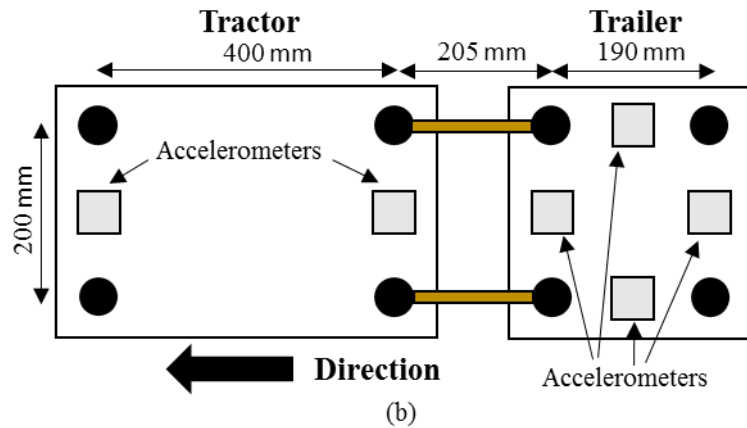
425 **Vehicle**

(a)

426

(b)

427
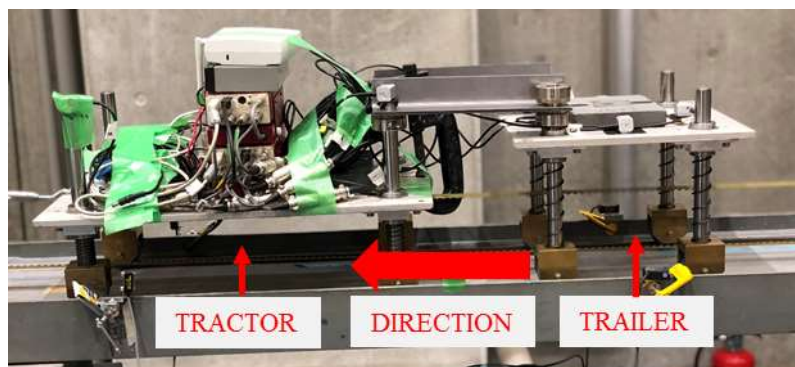
428 Fig. 10: (a) Experimental vehicle consisting of a tractor and trailer which are connected (b) Dimensions in plan
429 view of the vehicle

430 The vehicle used in the experiments is shown in Fig. 10(a). It consisted of a two-axle tractor,

431 connected to a two-axle trailer. Both the tractor and trailer consisted of sprung steel plates. The

432 front tractor axle had two springs of stiffness 1533 N m^{-1} and the rear axle had two springs of

433 stiffness 1753 N m^{-1}. The trailer had four equal axle suspension springs of stiffness 8464 N m^{-}

434 ^{1}. The tractor and trailer had axle spacings of 400 mm and 190 mm respectively and the spacing

435 between the rear tractor axle and front trailer axle was 205 mm (Fig. 10(b)).

436 The vehicle speed was kept constant by an electronic controller as it traversed the bridge.

437 Traversing speeds of 1.14 m/s and 1.26 m/s were used in this experiment. Two different tractor

438 masses, 24.3 kg and 26.3 kg were investigated to study potential sensitivity issues. The sprung

439 mass (i.e. the mass supported by springs) of the tractor for these two weights was 20.7 kg and

440 22.7 kg respectively. The trailer mass was 13.7 kg (of which 10.1 kg was sprung). The vehicle

441 was maintained on the bridge by two steel tracks, see Fig. 11. Accelerometers were installed

442 on the tractor and trailer in the locations shown in Fig. 10(b) which allows the vehicle

443 frequencies to be calculated. The tractor had bounce and pitch frequencies of 3.1 Hz and 4.7

444 Hz respectively (for the 20.7 kg case) and the trailer had bounce and pitch frequencies of 6.6

445 Hz and 3.5 Hz respectively. These were obtained using free vibration vehicle acceleration

446 measurements (after the vehicle has come to a halt) which were subsequently analysed using

447 Frequency Domain Decomposition (FDD) (Brincker et al., 2001), enabling the pitch and

448 bounce modes be distinguished.
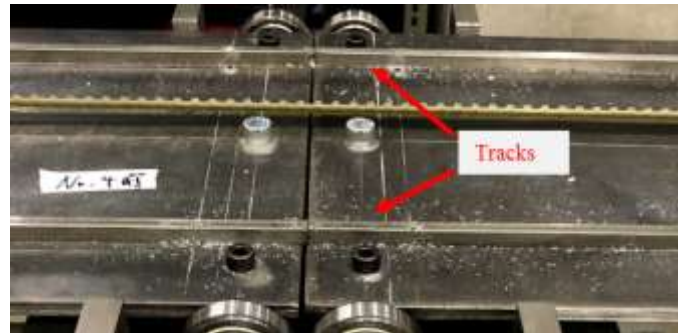
449

450 Fig. 11: Vehicle Tracks

Experimental Results

452 The concept of using relative pier mode shape amplitudes is introduced in a previous section

453 using theoretical mode shapes extracted from Eigen-analyses (Clough and Penzien, 1993) and

454 a brief numerical demonstration. In this section, the procedure is applied to the acceleration

455 signals generated at various points on a scaled bridge structure (see previous section) to

456 ascertain how successful the approach is when the modal information is extracted directly from

457 time signals incorporating natural experimental error.

Procedure

459 In the experimental tests, the model vehicle traversed the bridge at a specified velocity resulting

460 in four acceleration measurements from the midspans and three from the piers. The resulting

461 accelerations contain components relating to both the vehicle-induced vibrations and the

462 subsequent free vibration. The time-domain signals are analysed using FDD to identify the

463 mode shapes. Two vehicle speeds and tractor masses are investigated to ascertain how

464 experimental variation influences the results. The FDD processing is undertaken in the

465 MATLAB programming environment.

466 **Extraction of mode shapes for healthy case**
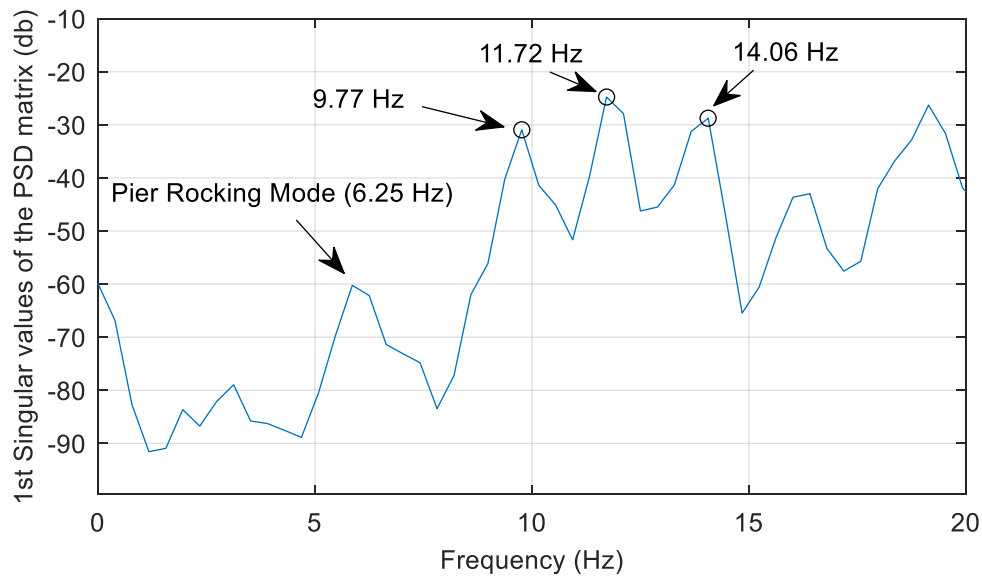
467

468 Fig. 12: Experimental FDD frequency picking from singular values of the spectral density matrix for vehicle
469   crossing at speed of 1.26 m/s (with tractor mass of 22.7 kg)

470 Fig. 12 shows the 1st singular values of the Power Spectral Density (PSD) matrix obtained by

471 applying FDD to the seven acceleration signals resulting from the vehicle (with tractor mass

472 of 22.7 kg) traversing the bridge at 1.26 m/s. As is evident, many peaks appear on the plot,

473 each corresponding to a different mode of vibration. To demonstrate the process of deriving

474 the mode shapes, three peaks are identified herein at 9.77 Hz, 11.72 Hz and 14.06 Hz. There is

475 also a smaller peak visible at 6.25 Hz, which correlates to a pier rocking mode. Fig. 13 shows

476 the extracted mode shapes corresponding to the three frequency peaks selected in Fig. 12. For

477 ease of visualisation, a spline curve is fitted to the extracted points.

478
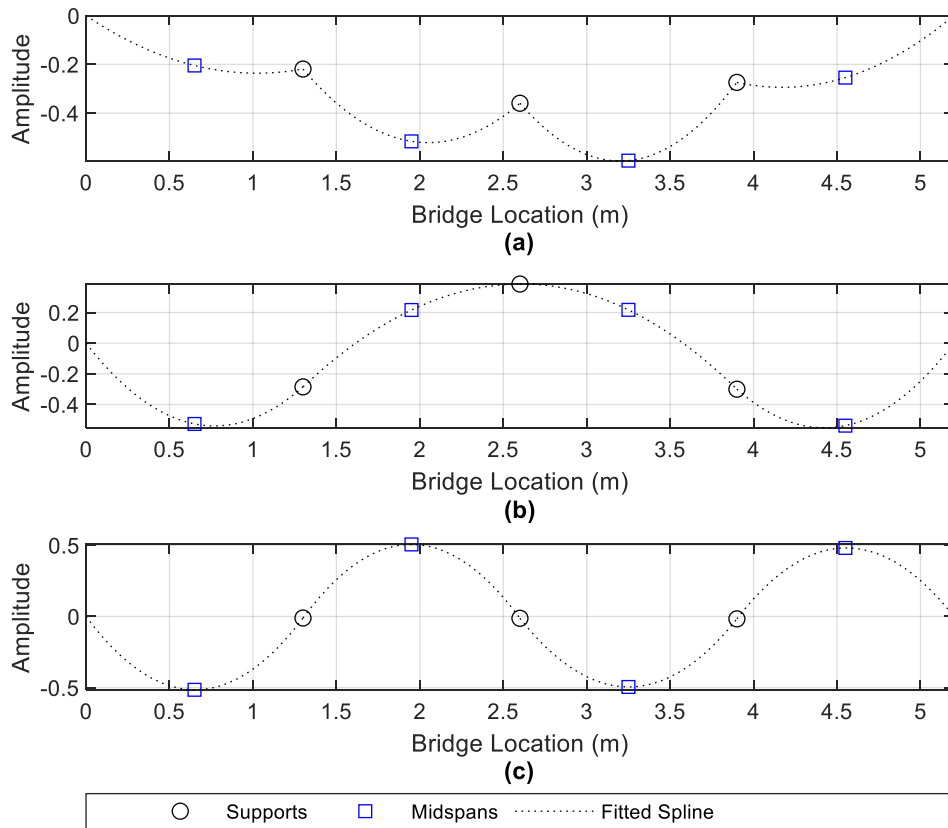
Fig. 13: Mode shapes derived from experimental accelerations - (a) 9.77 Hz mode, (b) 11.72 Hz mode, (c) 14.06
Hz mode

Fig. 13(a) shows the first mode of the structure, at a frequency of 9.77 Hz. This mode shape

resembles that of the numerical model of the full-scale structure shown in Fig. 2 in that all the

piers are moving in the same direction. This is the 'first' mode shape and is the primary focus

of the present work to detect a loss of stiffness due to scour. The 11.72 Hz mode (Fig. 13(b))

differs from the 9.77 Hz mode in that Pier 2 (the centre pier) is moving in a different direction

to Piers 1 and 3. Finally, in the 14.06 Hz mode (Fig. 13(c)), the piers exhibit negligible

movement in comparison to the midspans. Due to this, the 9.77 Hz and 11.72 Hz modes would

have an expected change due to scour but the 14.06 Hz mode would not (as the piers have

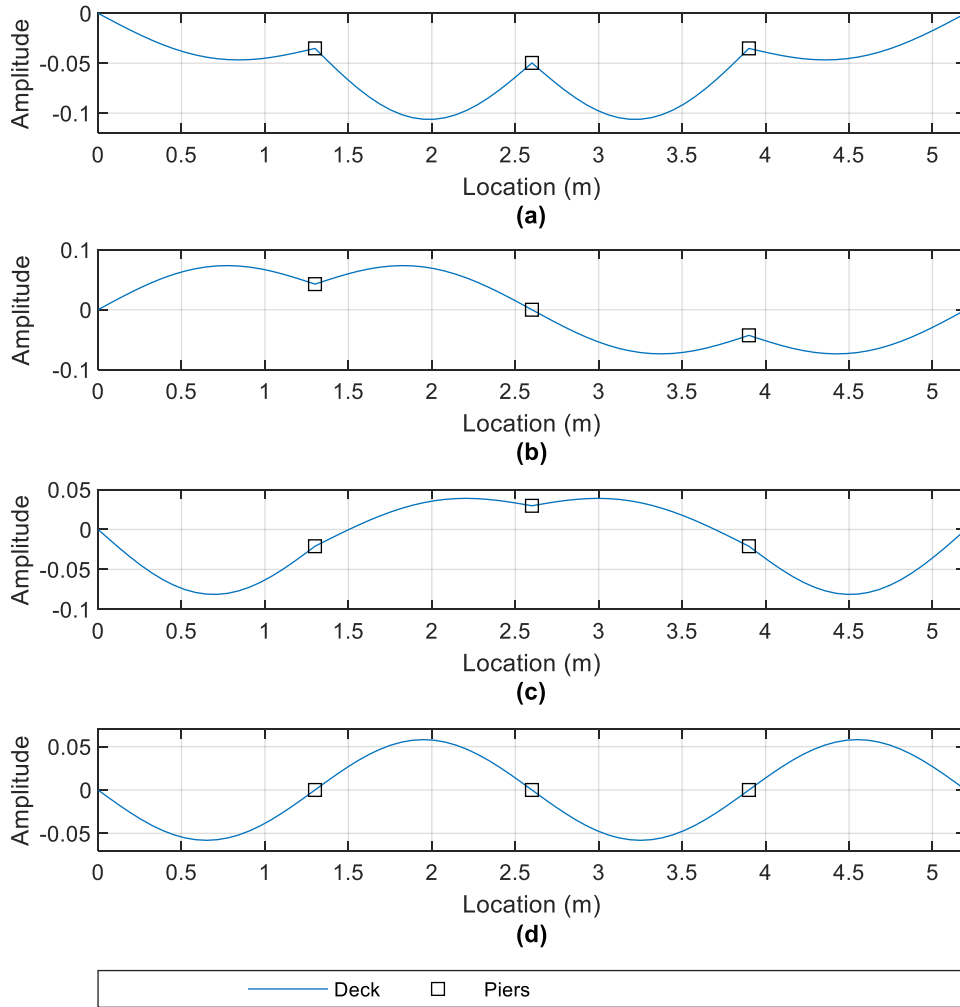insignificant modal amplitudes in this mode).

490

Fig. 14: First four mode shapes of system from numerical model - (a) 9.66 Hz mode, (b) 10.55 Hz mode, (c) 12.09 Hz mode, (d) 13.85 Hz mode

A numerical model of the scaled experimental arrangement is developed using the approach described previously and using the experimental parameters in Table 2. Fig. 14 shows the mode shapes of the first four frequencies derived from the numerical model by solving the Eigenproblem of the system matrices (Clough and Penzien, 1993). It is worth noting that the pier stiffness, k_{pier}, in the model is assumed to be infinite compared to the foundation stiffness, k_f. Here, the value of k_{pier} is selected by multiplying k_f by 10^4 (i.e. an arbitrary large number). The steel tracks are also included in the numerical model so the beam second moment of area and cross-sectional area are altered to account for this. With the tracks included, these properties are 21.67×10^3 mm^4 and 2549 mm^2 respectively.

27

502   A comparison of the experimental mode shapes (Fig. 13) derived from the time-domain

503   acceleration signals and the numerically calculated ones (with the experimental model

504   parameters - Fig. 14) shows clear similarities. The experimental and numerical modes of 9.77

505   Hz and 9.66 Hz (Figs. 13(a) and 14(a)), 11.72 Hz and 12.09 Hz (Figs. 13(b) and 14(c)) and

506   14.06 Hz and 13.85 Hz (Figs. 13(c) and 14(d)) show a clear correspondence, which provides a

507   reasonable level of confidence in the experimental results from the FDD algorithm. Given the

508   difficulties associated with accurately modelling the real experimental situation, the differences

509   in the frequencies between numerical and experimental cases are relatively minor. The

510   numerical mode of 10.55 Hz (Fig. 14(b)) is not sufficiently excited by the traversing model

511   vehicle in the experiment to show in the peak selection process in Fig. 12. Of note is the

512   frequency for the numerical mode in Fig. 14(d). The frequency of 13.85 Hz is the same as the

513   first natural frequency of a single span simply supported beam case. This is unsurprising as the

514   piers do not show any deflection in Fig. 14(d), equivalent to pinned supports.

515 **Extraction of mode shapes for scoured case**
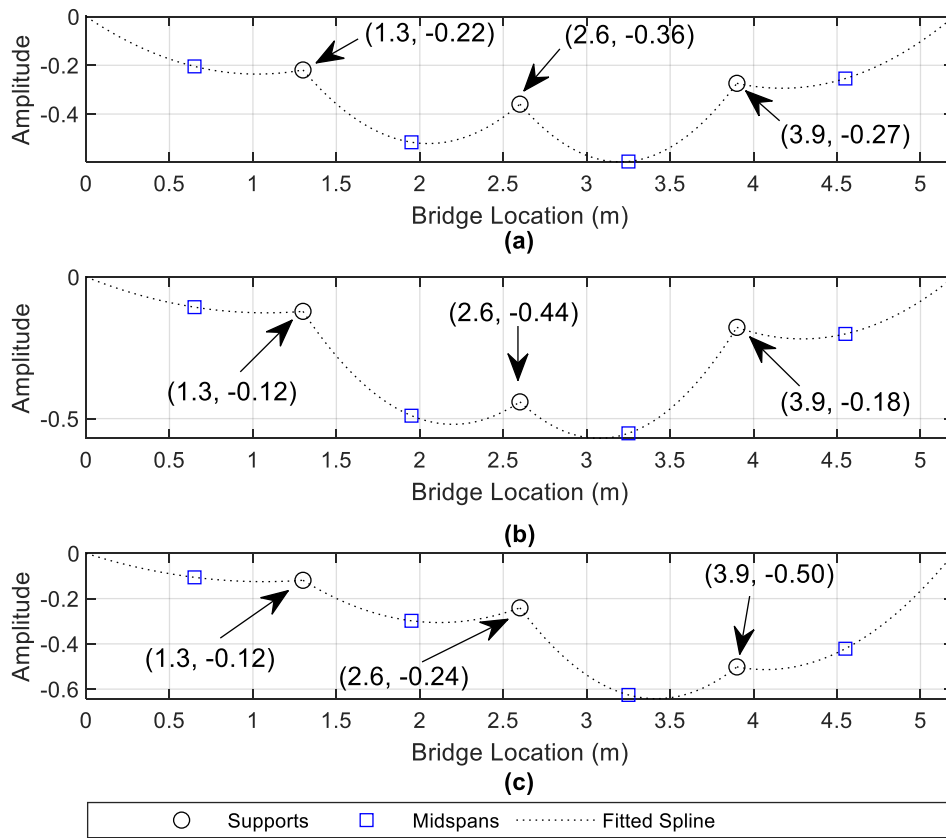
516

517   Fig. 15: First mode shape (derived from experimental accelerations) for different scour scenarios for vehicle
518   crossing at speed of 1.26 m/s (with a tractor mass of 22.7 kg) – (a) Healthy case, (b) 24.5 % stiffness loss at Pier
519   2, (c) 24.5 % stiffness loss at Pier 3

520   Fig. 15 shows how the first mode shape of the experimental bridge changes for the scour

521   scenarios equivalent to 24.5% stiffness loss at Pier 2 (with other piers remaining healthy) and

522   24.5% foundation stiffness loss at Pier 3 (with the other piers remaining healthy). For each

523   case, the change in mode shape amplitude is greatest at the location of the scoured pier. Table

524   3 shows the MNMS values which are defined in Eq. (2) for the scenarios in Fig. 15. The MNMS

525   value at the scoured pier increases due to scour stiffness loss while the MNMS values at the

526   other piers decrease. This generally corroborates the findings from the numerical study in a

527   previous section. Moreover, the percentage increases in the MNMS values are greater for the

528   case of scour at Pier 3 than at Pier 2 - 0.93 to 2.78 (198.9% increase) vs 1.47 to 2.93 (99.3%

529   increase). This is in line with the findings from the numerical study in that the MNMS value

530   increases more for stiffness loss at an off-centre pier than at the central pier.

531   Table 3: Experimental MNMS values calculated for 24.5% stiffness reduction (using values marked in Fig. 15)

Scour Condition	MNMS$_{Pier\ 1}$	MNMS$_{Pier\ 2}$	MNMS$_{Pier\ 3}$
Healthy	0.70	1.47	0.93
24.5% Scour Pier 2	0.39	2.93	0.64
24.5% Scour Pier 3	0.32	0.77	2.78

532

533   **Sensitivity of MNMS for different locations and severities of scour**

534   **considering vehicle condition variability**

535   Fig. 16 shows the MNMS values for scour at Pier 2 calculated from different vehicle runs for

536   a healthy case and stiffness losses due to scour of 24.5% and 44.9%. Two different tractor

537   masses and vehicle speeds are investigated with each repeated three times for each scenario.

538   The tractor masses tested are 24.3 kg and 26.3 kg, and the vehicle speeds are 1.14 m s^{-1} and

539   1.26 m s^{-1}. The MNMS values in Fig. 16 are shown relative to each vehicle run and the specific

540   conditions are shown below Fig. 16(c). The MNMS values are quite repeatable for each scour

541   case. This is not unexpected, as the indicators are based on a vibration mode of the structure,

542   so they should not be significantly affected by a change in vehicle parameters. The results for

543   the case considered (scour at Pier 2) show that the MNMS increases in value at the scoured

544   pier for the two scour magnitudes considered and decreases at the remaining piers (relative to

545   the healthy case).

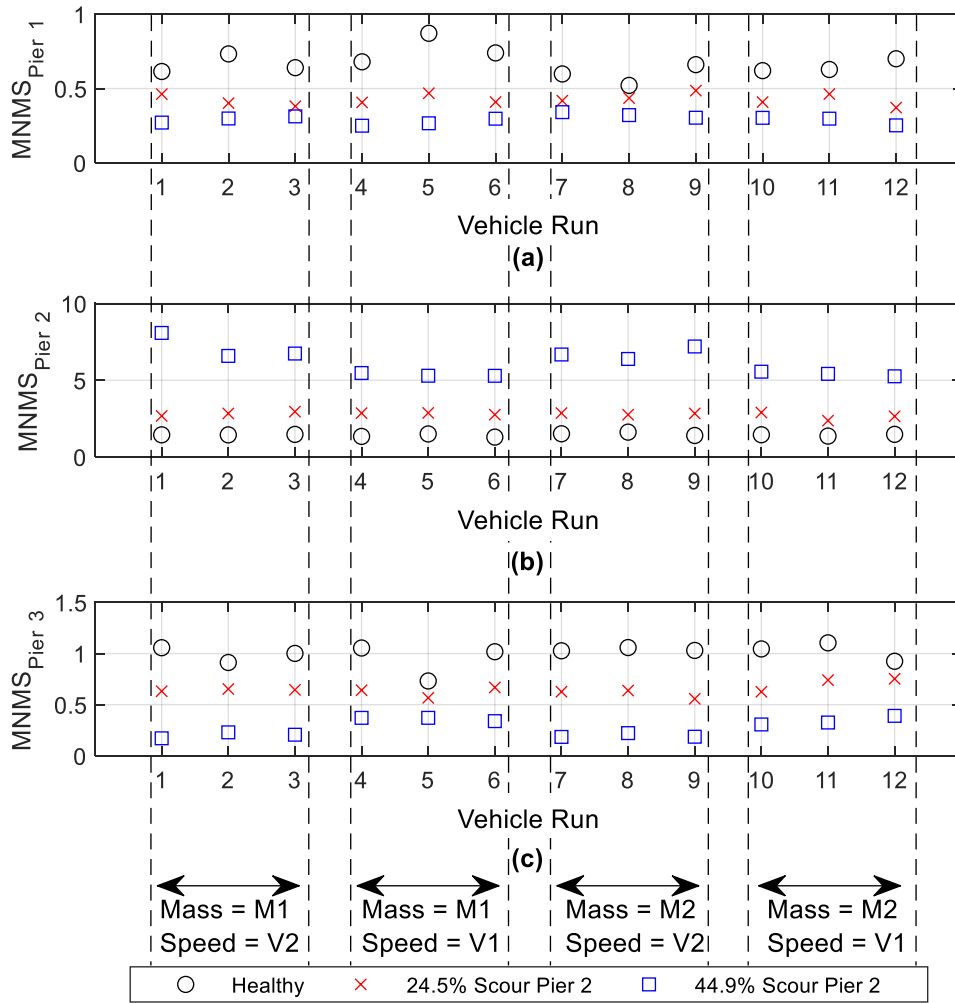Fig. 16: MNMS values for scour at Pier 2 repeated for multiple vehicle runs where M1 and M2 refer to tractor masses of 24.3 kg and 26.3 kg respectively and V1 and V2 refer to vehicle speeds of 1.14 m/s and 1.26 m/s respectively (a) $MNMS_{Pier1}$ (b) $MNMS_{Pier2}$ (c) $MNMS_{Pier3}$
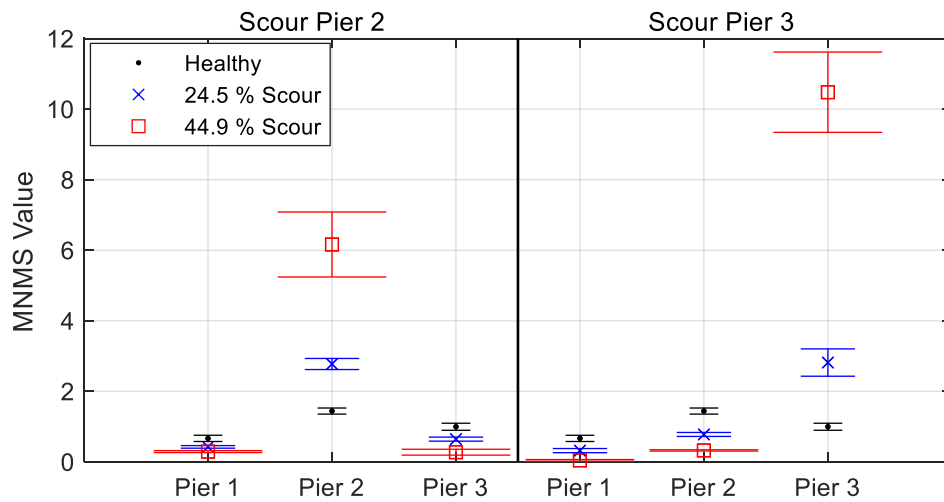

Fig. 17: Mean and one standard deviation error bar plots of scour scenarios at Pier 2 and Pier 3 for severities of 24.5% and 44.9%

31

553   Fig. 17 (left side) shows the mean of the MNMS values for the 12 runs considered in Fig. 16

554   +/- one standard deviation (shown by error bars on the plot). The same information is shown

555   on the right side of the plot for the case where the scour is at Pier 3. There is a clear distinction

556   between the regions defined by the error bars for each scour scenario. In other words, the error

557   bars do not overlap, which shows that the effect of scour outweighs any variability effects

558   (within 1 standard deviation) due to the vehicle changes considered or natural variability due

559   to measurement error. It can also be seen in Fig. 17 that the scale of the increases at the scoured

560   pier are far greater than the changes at the unscoured piers, making it clear which pier is scoured

561   for a given case. Similar to the findings in the numerical study, the MNMS experiences a

562   greater increase for off-centre piers than for central piers. This is shown in Fig. 17 for the 44.9%

563   scour case where there is a larger change in MNMS at Pier 3 for the case of scour at Pier 3 than

564   the change in the MNMS at Pier 2 for the case of scour at Pier 2.

Performance of MNMS against Modal Assurance Criterion (MAC)

566   The performance of the MNMS approach against traditional damage-detection methods based

567   on comparing healthy and damaged mode shapes using MAC is of interest. In this section, a

568   brief analysis is conducted to assess the relative performance of MNMS and MAC as indicators

569   of scour damage. The experimental results from vehicles crossing the model bridge are used to

570   derive the mode shapes for the case of the healthy bridge, and the bridge 'damaged' by scour

571   with stiffness reductions of 24.5% and 44.9% at Pier 2. In total, six crossing of the healthy

572   case, and six crossings for each of the two damage cases are used to obtain the mean values of

573   the mode shapes for each condition. MAC is defined as in Eq. (7)

$$\text{MAC} = \frac{\left|\Phi_{\text{healthy}}{}^{t}\Phi_{\text{damaged}}\right|^{2}}{\left|\Phi_{\text{healthy}}{}^{t}\Phi_{\text{healthy}}\right|\left|\Phi_{\text{damaged}}{}^{t}\Phi_{\text{damaged}}\right|} \tag{7}$$

574   where $\Phi_{healthy}$ is the mode shape obtained from the healthy bridge, $\Phi_{damaged}$ is the mode

575   shape obtained from the scoured bridge and "t" defines the matrix transpose. If the mode shapes

576   are identical, the MAC will have a value of one, but if they are very different, the MAC value

577   will be close to zero.

578   Table 4 shows the results of the MAC analysis. A MAC value of 0.9 between healthy and

579   damaged mode shapes is obtained for the case of 24.5% scour-related stiffness loss at Pier 2.

580   This reduces to 0.71 for an increased stiffness reduction to 44.9% at Pier 2. Table 5 shows the

581   MNMS derived for the same conditions. For 24.5% scour at P2, MNMS at P2 increases by

582   almost 100%, and decreases by 41% and 34% at P1 and P3 respectively. For 44.9% scour at

583   P2, MNMS at P2 increases by almost 341%, and decreases by 61% and 71% at P1 and P3

584   respectively relative to the zero scour case. From this analysis, it can be seen that MNMS is

585   more sensitive to scour damage than MAC, and moreover the location of scour can be detected

586   by observing the relative changes in the MNMS value at each pier. MNMS is potentially a

587   better indicator than the traditional MAC value for scour type damage detection.

588   Table 4 MAC Analysis

Case	Modal Amplitudes (-)			MAC
	Pier 1	Pier 2	Pier 3	
Healthy	-0.23	-0.36	-0.28	-
24.5% Scour	-0.14	-0.45	-0.19	0.9
44.9% Scour	-0.10	-0.62	-0.10	0.71

589

590   Table 5 MNMS Analysis

Case	MNMS$_{P1}$	% Change	MNMS$_{P2}$	% Change	MNMS$_{P3}$	% Change
Healthy	0.71	-	1.41	-	0.96	-
24.5% Scour	0.42	-41	2.82	100	0.63	-34
44.9% Scour	0.28	-60	6.24	341	0.28	-71

591

592 **Conclusions**

593 This paper presents an approach to detect stiffness loss arising due to scour based on relative

594 changes of vertical pier mode shape amplitudes. The method is tested using a scaled

595 experimental model of a bridge traversed by a vehicle. The experimental mode shapes are

596 extracted from acceleration signals arising due to the vehicle crossing using an output only

597 modal identification technique, namely Frequency Domain Decomposition. A scour

598 monitoring feature (MNMS) is defined, based on the first global mode shape of the structure

599 and is shown to increase significantly at a scoured pier. At the location of the scoured pier the

600 magnitude of the MNMS also increases with scour severity, suggesting that progressive scour

601 development could potentially be monitored. As the algorithm used is an output-only one, it

602 has the advantage of negating the requirement of knowing any details about the vehicle

603 excitation forces. Furthermore, material and geometrical information about the bridge such as

604 second moment of area or density, do not need to be known in order to apply the method.

605 Repeated vehicle runs to excite the bridge allow the MNMS to be derived and monitoring

606 changes in this metric alone can potentially detect scour. In practice, an initial visual inspection

607 of the bridge may help to determine the scour condition at the time of instrumentation, and this

608 would be the benchmarked 'unscoured' case. Once instrumented, the bridge can potentially be

609 monitored on a continual basis using the method proposed in this paper.

610 It should be noted that while scour is the target damage in the present study, other forms of

611 damage such as concrete spalling or corrosion will also lead to changes in stiffness of a

612 structure. Separating the scour influence from other damage types is challenging, however by

613 the very nature of scour occurring at supports, the relative changes in stiffness due to scour are

614 expected to be larger than would arise under other damage types. Additionally, if the MNMS

615 were to detect some form of stiffness loss (from scour or otherwise), this could be used to

616 trigger a manual visual inspection. It is therefore not so important to separate scour from other

617   damage as the end result for a bridge manager is to detect any issues arising in the structure to

618   facilitate the safe management of the asset.

619   The analysis in this paper considers scour at only one pier at a time to demonstrate the approach.

620   Scour at multiple piers simultaneously can cause issues with the method as it is derived using

621   the sum of the modal amplitudes at all piers to identify scour at a given affected pier. The

622   method therefore does not work well when scour affects multiple piers of a bridge

623   simultaneously. However, due to asymmetry in water-flow characteristics across a river

624   channel cross-section, it is unlikely for temporal scour development to be equal at multiple

625   piers, therefore the approach should still be capable of identifying scour occurrence once it

626   begins at a given pier.

627   While the approach was successfully demonstrated with an experimental scaled bridge in the

628   present study, a full-scale deployment is recommended before firm conclusions on the efficacy

629   of the method can be made. This is due to the natural differences that arise between $1g$ scaled

630   experimental testing and full-scale applications.

631   The approach described in this paper is novel in terms of bridge scour detection and will be

632   beneficial to the evolving vibration-based scour monitoring field.

Data Availability Statement

634   Some or all data, models, or code that support the findings of this study are available from the

635   corresponding author upon reasonable request. (Experimental Data.)

Acknowledgements

References

639

640   Allemang, R. J. & D. L. Brown. 1982. "A correlation coefficient for modal vector analysis".

641   *Proceedings of the 1st International Modal Analysis Conference*, 110-116.

642   Bao, T. & Z. Liu. 2017. "Vibration-based bridge scour detection: A review". *Structural*

643   *Control and Health Monitoring*, 24(7), e1937.

644   Bao, T., R. A. Swartz, S. Vitton, Y. Sun, C. Zhang & Z. Liu. 2017. "Critical insights for

645   advanced bridge scour detection using the natural frequency". *Journal of Sound and*

646   *Vibration*, 386, 116-133.

647   Briaud, J. L., S. Hurlebaus, K. A. Chang, C. Yao, H. Sharma, O. Y. Yu, C. Darby, B. E. Hunt

648   & G. R. Price, 2011. *Realtime monitoring of bridge scour using remote monitoring*

649   *technology*, Texas A&M University System, Texas.

650   Briaud, J. L., Z. Medina-Cetina, S. Hurlebaus, M. Everett, S. Tucker, N. Yousefpour & R.

651   Arjwech, 2012. *Unknown foundation determination for scour*, Texas Transportation

652   Institute, Texas.

653   Brincker, R., L. Zhang & P. Andersen. 2001. "Modal identification of output-only systems

654   using frequency domain decomposition". *Smart Materials and Structures*, 10(3), 441-

655   445.

656   Carden, E. P. & P. Fanning. 2004. "Vibration based condition monitoring: a review".

657   *Structural Health Monitoring*, 3(4), 355-377.

658   Chen, C. C., W. H. Wu, F. Shih & S. W. Wang. 2014. "Scour evaluation for foundation of a

659   cable-stayed bridge based on ambient vibration measurements of superstructure".

660   *NDT & E International*, 66, 16-27.

661   Clough, R. W. & J. Penzien 1993. *Dynamics of Structures*, McGraw-Hill.

662   Davis, N. T., E. Hoomaan, M. Sanayei, A. K. Agrawal & F. Jalinoos. 2018. "Integrated

663   Superstructure-Substructure Load Rating for Bridges with Foundation Movements".

664   *Journal of Bridge Engineering*, 23(5), 04018022.

665   Dos Santos, J. A., C. M. Soares, C. M. Soares & H. Pina. 2000. "A damage identification

666   numerical model based on the sensitivity of orthogonality conditions and least squares

667   techniques". *Computers & Structures*, 78(1-3), 283-291.

668   Elsaid, A. & R. Seracino. 2014. "Rapid assessment of foundation scour using the dynamic

669   features of bridge superstructure". *Construction and Building Materials*, 50, 42-49.

670   Fan, W. & P. Qiao. 2011. "Vibration-based damage identification methods: a review and

671   comparative study". *Structural Health Monitoring*, 10(1), 83-111.

672   FEMA, 2000. *Prestandard and commentary for the seismic rehabilitation of buildings -

673   Report FEMA-356*, Washington, DC.

674   Fitzgerald, P. C., A. Malekjafarian, B. Bhowmik, L. J. Prendergast, P. Cahill, C. W. Kim, B.

675   Hazra, V. Pakrashi & E. J. OBrien. 2019a. "Scour Damage Detection and Structural

676   Health Monitoring of a Laboratory-Scaled Bridge Using a Vibration Energy

677   Harvesting Device". *Sensors*, 19(11), 2572.

678   Fitzgerald, P. C., A. Malekjafarian, D. Cantero, E. J. OBrien & L. J. Prendergast. 2019b.

679   "Drive-by scour monitoring of railway bridges using a wavelet-based approach".

680   *Engineering Structures*, 191, 1-11.

681   Forde, M., D. Mccann, M. Clark, K. Broughton, P. Fenning & A. Brown. 1999. "Radar

682   measurement of bridge scour". *NDT & E International*, 32(8), 481-492.

683   Foti, S. & D. Sabia. 2010. "Influence of foundation scour on the dynamic response of an

684   existing bridge". *Journal of Bridge Engineering*, 16(2), 295-304.

685   Frýba, L. & M. Pirner. 2001. "Load tests and modal analysis of bridges". *Engineering

686   Structures*, 23(1), 102-109.

687   Hamill, L. 1999. *Bridge Hydraulics,* Routledge, London & New York, E.& F.N. Spon.

688   Hardin, B. O. & V. P. Drnevich. 1972. "Shear Modulus and Damping in Soils: Design

689   Equations and Curves". *Journal of the Soil Mechanics and Foundations Division*,

690   98(7), 667-692.

691   Ju, S. 2013. "Determination of scoured bridge natural frequencies with soil–structure

692   interaction". *Soil Dynamics and Earthquake Engineering*, 55, 247-254.

693   Keenahan, J., E. J. OBrien, P. J. Mcgetrick & A. Gonzalez. 2013. "The use of a dynamic

694   truck-trailer drive-by system to monitor bridge damping". *Structural Health*

695   *Monitoring*, 13(2), 143-157.

696   Khatibi, M., M. Ashory, A. Malekjafarian & R. Brincker. 2012. "Mass–stiffness change

697   method for scaling of operational mode shapes". *Mechanical Systems and Signal*

698   *Processing*, 26, 34-59.

699   Klinga, J. V. & A. Alipour. 2015. "Assessment of structural integrity of bridges under

700   extreme scour conditions". *Engineering Structures*, 82, 55-71.

701   Kong, X. & C. S. Cai. 2016. "Scour Effect on Bridge and Vehicle Responses under Bridge–

702   Vehicle–Wave Interaction". *Journal of Bridge Engineering*, 21(4), Article ID

703   04015083.

704   Kong, X., C. S. Cai & S. Hou. 2013. "Scour effect on a single pile and development of

705   corresponding scour monitoring methods". *Smart Materials and Structures*, 22(5),

706   Article ID 055011.

707   Kong, X., C. S. Cai & J. Hu. 2017. "The state-of-the-art on framework of vibration-based

708   structural damage identification for decision making". *Applied Sciences*, 7(5), 497.

709   Kwon, Y. W. & H. Bang 2000. *The finite element method using MATLAB,* Boca Raton,

710   Florida, CRC press.

711   Maddison, B. 2012. "Scour failure of bridges". *Proceedings of the Institution of Civil*

712   *Engineers-Forensic Engineering*, 165(1), 39-52.

713   Malekjafarian, A. & E. J. OBrien. 2014. "Identification of bridge mode shapes using short

714   time frequency domain decomposition of the responses measured in a passing

715   vehicle". *Engineering Structures*, 81, 386-397.

716   Malekjafarian, A. & E. J. OBrien. 2017. "On the use of a passing vehicle for the estimation of

717   bridge mode shapes". *Journal of Sound and Vibration*, 397, 77-91.

718   Moughty, J. J. & J. R. Casas. 2017. "A state of the art review of modal-based damage

719   detection in bridges: Development, challenges, and solutions". *Applied Sciences*, 7(5),

720   510.

721   Mylonakis, G., S. Nikolaou & G. Gazetas. 2006. "Footings under seismic loading: Analysis

722   and design issues with emphasis on bridge foundations". *Soil Dynamics and*

723   *Earthquake Engineering*, 26(9), 824-853.

724   OBrien, E. J., P. C. Fitzgerald, A. Malekjafarian & E. Sevillano. 2017. "Bridge damage

725   detection using vehicle axle-force information". *Engineering Structures*,

726   153(Supplement C), 71-80.

727   OBrien, E. J. & A. Malekjafarian. 2016. "A mode shape-based damage detection approach

728   using laser measurement from a vehicle crossing a simply supported bridge".

729   *Structural Control and Health Monitoring*, 23(10), 1273-1286.

730   Oztoprak, S. & M. Bolton. 2013. "Stiffness of sands through a laboratory test database".

731   *Géotechnique*, 63(1), 54-70.

732   Pais, A. & E. Kausel. 1988. "Approximate formulas for dynamic stiffnesses of rigid

733   foundations". *Soil Dynamics and Earthquake Engineering*, 7(4), 213-227.

734   Pandey, A., M. Biswas & M. Samman. 1991. "Damage detection from changes in curvature

735   mode shapes". *Journal of Sound and Vibration*, 145(2), 321-332.

736   Prendergast, L. J. & K. Gavin. 2014. "A review of bridge scour monitoring techniques".

737   *Journal of Rock Mechanics and Geotechnical Engineering*, 6(2), 138-149.

738   Prendergast, L. J. & K. Gavin. 2016. "A comparison of initial stiffness formulations for

739   small-strain soil–pile dynamic Winkler modelling". *Soil Dynamics and Earthquake*

740   *Engineering*, 81, 27-41.

741   Prendergast, L. J., K. Gavin & D. Hester. 2017. "Isolating the location of scour-induced

742   stiffness loss in bridges using local modal behaviour". *Journal of Civil Structural*

743   *Health Monitoring*, 7(4), 483-503.

744   Prendergast, L. J., D. Hester & K. Gavin. 2016a. "Determining the presence of scour around

745   bridge foundations using vehicle-induced vibrations". *Journal of Bridge Engineering*,

746   21(10), Article ID 04016065.

747   Prendergast, L. J., D. Hester & K. Gavin, 2016b. Development of a vehicle-bridge-soil

748   dynamic interaction model for scour damage modelling. *Shock and Vibration*. DOI:

749   10.1155/2016/7871089

750   Prendergast, L. J., D. Hester, K. Gavin & J. O'Sullivan. 2013. "An investigation of the

751   changes in the natural frequency of a pile affected by scour". *Journal of Sound and*

752   *Vibration*, 332(25), 6685-6702.

753   Prendergast, L. J., M. P. Limongelli, N. Ademovic, A. Anzlin, K. Gavin & M. A. Zanini.

754   2018. "Structural Health Monitoring for Performance Assessment of Bridges under

755   Flooding and Seismic Actions". *Structural Engineering International*, 28(3), 296-307.

756   Ratcliffe, C. P. 2000. "A frequency and curvature based experimental method for locating

757   damage in structures". *Journal of Vibration and Acoustics*, 122(3), 324-329.

758   Salawu, O. S. & C. Williams. 1995. "Bridge assessment using forced-vibration testing".

759   *Journal of Structural Engineering*, 121(2), 161-173.

760   Scozzese, F., L. Ragni, E. Tubaldi & F. Gara. 2019. "Modal properties variation and collapse

761   assessment of masonry arch bridges under scour action". *Engineering Structures*, 199,

762   109665.

763   Sohn, H. 2006. "Effects of environmental and operational variability on structural health

764   monitoring". *Philosophical Transactions of the Royal Society A: Mathematical,*

765   *Physical and Engineering Sciences*, 365(1851), 539-560.

766   Sohn, H., C. R. Farrar, F. M. Hemez, D. D. Shunk, D. W. Stinemates, B. R. Nadler & J. J.

767   Czarnecki. 2003. "A review of structural health monitoring literature: 1996–2001".

768   *Los Alamos National Laboratory, USA*.

769   Wahab, M. A. & G. De Roeck. 1999. "Damage detection in bridges using modal curvatures:

770   application to a real damage scenario". *Journal of Sound and Vibration*, 226(2), 217-

771   235.

772   Wardhana, K. & F. C. Hadipriono. 2003. "Analysis of recent bridge failures in the United

773   States". *Journal of Performance of Constructed Facilities*, 17(3), 144-150.

774   Xiong, W., C. Cai, B. Kong, P. Tang & J. Ye. 2018a. "Identification of bridge scour depth by

775   tracing dynamic behaviors of superstructures". *KSCE Journal of Civil Engineering*,

776   22(4), 1316-1327.

777   Xiong, W., C. Cai, B. Kong, X. Zhang & P. Tang. 2019. "Bridge Scour Identification and

778   Field Application Based on Ambient Vibration Measurements of Superstructures".

779   *Journal of Marine Science and Engineering*, 7(5), 121.

780   Xiong, W., B. Kong, P. Tang & J. Ye. 2018b. "Vibration-Based Identification for the

781   Presence of Scouring of Cable-Stayed Bridges". *Journal of Aerospace Engineering*,

782   31(2), 04018007.

783   Zhang, H., S. Chen & F. Liang. 2017. "Effects of scour-hole dimensions and soil stress

784   history on the behavior of laterally loaded piles in soft clay under scour conditions".

785   *Computers and Geotechnics*, 84, 198-209.

786   Zhu, X. Q. & S. S. Law. 2002. "Moving loads identification through regularization". *Journal*

787   *of Engineering Mechanics*, 128(9), 989-1000.

788